Large-eddy simulation of the injection timing effects on the dual-fuel spray flame

Xu, Shijie; Zhong, Shenghui ; Hadadpour, Ahmad; Zhang, Yan; Pang, Kar Mun; Jangi, Mehdi; Fatehi, Hesameddin; Bai, Xue Song

DOI:
10.1016/j.fuel.2021.122445

Fuel 310 (2022) 122445

Contents lists available at ScienceDirect

Fuel

journal homepage: www.elsevier.com/locate/fuel

Full length article

Large-eddy simulation of the injection timing effects on the dual-fuel spray flame

Shijie Xu [a,*], Shenghui Zhong [a,b], Ahmad Hadadpour [a], Yan Zhang [a,b], Kar Mun Pang [c], Mehdi Jangi [d], Hesameddin Fatehi [a], Xue-Song Bai [a]

[a] Department of Energy Sciences, Lund University, 22100 Lund, Sweden
[b] State Key Laboratory of Engines, Tianjin University, 135 Yaguan Rd, 300350 Tianjin, PR China
[c] MAN Energy Solutions, Teglholmsgade 41, 2450 Copenhagen SV, Denmark
[d] School of Mechanical Engineering, University of Birmingham, Edgbaston, Birmingham B15 2TT, UK

ARTICLE INFO

Keywords:
Large eddy simulation
Dual-fuel combustion
Engine Combustion Network
Ignition
Injection timing

ABSTRACT

Large-eddy simulations (LES) coupled with a partially-stirred reactor model and a finite-rate chemistry are carried out to investigate the effects of n-heptane injection timing on the methanol fueled dual-fuel (DF) combustion. Methanol is premixed with air in a constant volume chamber (T=1000 K, ρ=14.8 kg/m^3) to form a homogeneous mixture (equivalence ratio ϕ_m of 0.3). Liquid fuel n-heptane is provided from a high pressure injector to mimic the pilot fuel injection in DF engines. First, mesh sensitivity analysis and LES model validation are conducted. The experimental data of Spray-H (n-heptane fueled) from the Engine Combustion Network is used for model validation. It is shown that the present mesh and LES model are capable of replicating the liquid and vapor penetration length, mixture fraction, temperature distribution, pressure rise profile and ignition delay time (IDT). Second, the effects of n-heptane injection timing are investigated, by varying the start of injection (SOI) time. The LES results reveal that there are three stage heat releases in the DF combustion. With the delay of SOI, the mass fraction of hydrogen peroxide in the ambient mixture increases, leading to an early formation of hydroxyl. Therefore, the two-stage IDTs of n-heptane decrease, while the ambient methanol IDT increases. Results also show the cool flame and high-temperature flame evolution after methanol auto-ignition. The cool flame disappears while the high-temperature flame is found near the injector nozzle, which leads to a relatively high heat release rate.

1. Introduction

With the increasing demand of energy and concern on pollutant emissions, the use of alternative renewable fuels is in focus for internal combustion engines (ICE). As one of the ideal alternative fuels, methanol has attracted attention due to its rich resources and clean combustion features. Methanol can be produced from fossil fuels, e.g., coal, petroleum and natural gas [1]. It may also be produced from renewable sources, such as biomass, or carbon dioxide from industrial effluents or the atmosphere through reductive conversion with hydrogen [2]. It is desirable to use methanol as fuel for compression–ignition (CI) engines [3], which are widely used and have higher thermal efficiency. Methanol has a high latent heat value, which reduces the in-cylinder temperature of methanol-fueled engines [4], thus, in favor of reducing nitrogen oxide (NOx). As an oxygenated fuel without carbon–carbon bonds, methanol has a tendency of not only low soot formation but also enhanced soot oxidation [5]. The use of methanol in CI engines can reduce soot and NOx emissions [5,6]. However, there are challenges in using methanol directly in CI engines. Pure methanol is difficult to be ignited in conventional CI engines, in particular under low-load or cold-start conditions. The ignition delay time (IDT) of methanol is longer compared to conventional diesel. This may cause incomplete combustion and misfire [7].

Dual-fuel (DF) combustion strategy has been proposed to overcome methanol auto-ignition difficulties. In DF engines, a primary fuel with long IDT and a pilot fuel with short IDT are introduced into the engine separately. A typical diesel/methanol heavy-duty DF engine has two fuel tanks. Methanol is served as the primary fuel, premixed with air through port injection, while diesel is injected as the pilot fuel in the later compression stroke to ignite the premixed methanol/air mixture [8]. The timing of the main heat release from the primary fuel combustion is expected near the top-dead-center (TDC) to achieve a better thermal efficiency. An early pilot fuel injection timing gives

* Corresponding author.
E-mail address: shijie.xu@energy.lth.se (S. Xu).

https://doi.org/10.1016/j.fuel.2021.122445
Received 5 August 2021; Received in revised form 5 October 2021; Accepted 27 October 2021
Available online 18 November 2021

Table 1
Physical and chemical properties of methane, methanol, n-heptane and n-dodecane [5,23,24].

	Methane	Methanol	n-heptane	n-dodecane
Formula	CH_4	CH_3OH	C_7H_{16}	$C_{12}H_{26}$
Molecular weight (g/mol)	16	32	100	170
Density (kg/m^3, at 20 °C)	0.66	790	680	750
Cetane number	–	–	56	83
Octane number	108	120	–	–
Auto-ignition temperature (°C)	537	470	215	204
Lower heating value (MJ/kg)	50.05	20.27	44.92	44.57

rise to a high heat release rate (HRR) before the TDC, resulting in a reduction of power output and/or engine knock [9]. In contrast, a late injection leads to high hydrocarbon (HC) and carbon monoxide (CO) emissions [10]. Thus, a precise control of the pilot fuel injection timing is desirable in DF combustion strategy.

The pilot fuel ignition and combustion characteristics play a key role in the injection timing control. However, different from the single-fuel (SF) combustion in conventional CI engines, the ambient primary fuel in the DF combustion is reactive and interacts with the reactions of the pilot fuel. Studies on the interaction between primary fuels and pilot fuels have recently attracted the attention of various researchers [11–18]. Table 1 shows the physical and chemical properties of methane, methanol and diesel surrogate fuels n-dodecane and n-heptane. Srna et al. [11,12] conducted DF spray combustion experiments in a rapid compression–expansion machine, in which optical diagnostics were carried out to characterize n-dodecane (pilot fuel) spray ignition in an ambient methane/air mixture. It was shown that the n-dodecane IDT and combustion duration were prolonged in the presence of ambient methane. Kahila et al. [14,15] also observed a similar IDT retardation behavior of n-dodecane/methane DF combustion in their numerical studies. They suggested that both the low-temperature stage and high-temperature stage ignitions of the pilot fuel (n-dodecane) are retarded due to the chemical reactions in ambient methane/air mixture. Compared to methane, methanol exhibits a stronger retarding effect on the pilot fuel IDTs [19,20]. Karimkashi et al. [17] carried out zero-dimensional simulations to study the ignition properties of methane–diesel and methanol–diesel mixtures in a constant volume homogeneous reactor. It was reported that the ignition potential in methanol–diesel mixture is lower than that in the corresponding methane case. Gadalla et al. [21] studied diesel spray-assisted ignition of methanol–hydrogen blends using both zero-dimensional simulations and large-eddy simulations (LES). An ignitability map was proposed and suggested that DF diesel/methanol system has a narrow temperature window for smooth ignition. In a recent LES study of n-heptane/methanol DF combustion [22], it was also found that n-heptane ignition is retarded in the atmosphere of methanol. Under low ambient temperatures, the retardation effect is more pronounced and the IDT is longer, which extends the mixing time. A longer mixing time results in a lower local equivalence ratio and thus lower soot emission. Therefore, the change of the pilot fuel ignition and combustion characteristics should be taken into account to recalculate the injection timing, especially in methanol-fueled DF engines.

In typical diesel/methanol DF heavy-duty engines, methanol is injected in the intake stroke, evaporated to be gaseous phase and premixed with air prior to the diesel injection. The start of injection (SOI) of diesel is near the end of the compression stroke [25]. Wang et al. [26] suggested that the ignition timing is closely related to the SOI. With an advanced SOI, the diesel ignition is retarded. With a late SOI, the ambient methanol could be auto-ignited before diesel injection, especially under high temperature conditions. This implies that the self-ignition behavior of the ambient mixture prior to pilot fuel injection cannot be ignored. Under engine conditions, the ambient gas compositions have changed, producing intermediate species during the time before SOI, i.e., the ignition induction time (IT). Wei et al. [18] simulated the n-heptane spray in a methane fumigated environment under engine-like conditions. It was reported that n-heptane ignition reactions were affected by the intermediate species formaldehyde (CH_2O), which was formed during the IT in the ambient methane/air mixture. Extending the IT leads to a higher CH_2O concentration and a shorter n-heptane IDT. It is worth mentioning that methanol has a lower octane number than methane (research octane number of 108 for methanol and 120 for methane) [27,28], implying more significant IT effects. To the best of the authors' knowledge, detailed numerical simulations of methanol IT effects on DF combustion are yet to be carried out.

Set against these backgrounds, the IT effects on n-heptane/methanol DF combustion are studied in the present study. LES is carried out as it can provide information about the local flow structure in detail, which is required to understand the DF ignition and flame structures. The case setup is based on the Engine Combustion Network (ECN) [29] Spray-H experiment, which provides a reference operating condition and model validation. A non-reacting spray and a reacting spray SF cases are first simulated, where n-heptane is fueled in a constant volume chamber. These LES results are validated using the associated measurements. Once the numerical model is validated, five DF cases with IT ranging from 0 to 1.2 ms are conducted to examine the IT effects on n-heptane IDT and DF flame structures. Such workflow is designed to gain an improved understanding of IT mechanism and optimize the ignition timing in DF combustion.

2. Mathematical formulation and numerical methods

2.1. Mathematical formulation

The Eulerian–Lagrangian approach is used to study two-phase flow. In the Eulerian framework, the gas phase is governed by continuity, momentum, species, and energy equations, which are described in LES formulation by Eqs. (1)–(4), respectively.

$$\frac{\partial \overline{\rho}}{\partial t} + \nabla \cdot \left(\overline{\rho}\tilde{\mathbf{U}}\right) = \overline{S}_{\rho}, \tag{1}$$

$$\frac{\partial \overline{\rho}\tilde{\mathbf{U}}}{\partial t} + \nabla \cdot \left(\overline{\rho}\tilde{\mathbf{U}}\tilde{\mathbf{U}}\right) = \nabla \cdot \left(\overline{\rho}\tilde{\mathbf{U}}\tilde{\mathbf{U}} - \overline{\rho\mathbf{U}\mathbf{U}}\right) - \nabla\overline{p} + \nabla \cdot \overline{\boldsymbol{\tau}} + \overline{\mathbf{S}}_{u}, \tag{2}$$

$$\frac{\partial \overline{\rho}\tilde{Y}_i}{\partial t} + \nabla \cdot \left(\overline{\rho}\tilde{\mathbf{U}}\tilde{Y}_i\right) = \nabla \cdot \left(\overline{\rho}\tilde{\mathbf{U}}\tilde{Y}_i - \overline{\rho\mathbf{U}Y_i}\right) - \nabla \cdot \left(\overline{\rho}\tilde{D}\nabla\tilde{Y}_i\right) + \overline{\rho}\widetilde{\dot{\omega}}_{Y_i} + \overline{S}_{Y_i}, \tag{3}$$

$$\frac{\partial \overline{\rho}\tilde{h}}{\partial t} + \nabla \cdot \left(\overline{\rho}\tilde{\mathbf{U}}\tilde{h}\right) = \nabla \cdot \left(\overline{\rho}\tilde{\mathbf{U}}\tilde{h} - \overline{\rho\mathbf{U}h}\right) + \frac{D\overline{p}}{Dt} + \nabla \cdot \left(\overline{\rho}\tilde{D}\nabla\tilde{h}\right) + \overline{\rho}\widetilde{\dot{\omega}}_{h} + \overline{S}_{h}, \tag{4}$$

where $\bar{\cdot}$ and $\tilde{\cdot}$ represent the LES spatial filtering and Favre averaging, respectively. ρ is density. $\mathbf{U}$ is velocity vector. Y_i is the ith species mass fraction. h is sensible enthalpy. p and τ denote pressure and stress tensor obtained from the resolved strain rate, respectively. $\dot{\omega}$ are the chemical reaction source terms while S represent spray source terms. For simplicity, the unity Lewis number assumption is adopted in species and energy equations. The first terms on the RHS of Eqs. (2)–(4) represent the sub-grid scale (SGS) effects.

In the Lagrangian framework, the liquid phase is represented and tracked by a large number of parcels, i.e., the so called Lagrangian particle tracking (LPT) approach. The governing equation for each parcel reads as

$$\frac{d}{dt}\mathbf{u}_p = \frac{C_D}{\tau_p}\frac{Re_p}{24}\left(\mathbf{u}_g - \mathbf{u}_p\right). \tag{5}$$

In this equation, $\mathbf{u}_p$ and $\mathbf{u}_g$ are parcel and surrounding gas velocity vectors, respectively; Re_p and τ_p are the Reynolds number and characteristic time of the parcel. C_D is the drag coefficient. More details are given in Section 2.2 and Ref. [30].

Table 2
Numerical methods and models in use.

	Models
Primary and secondary break-up	Rosin–Rammler and KH–RT [36]
Heat transfer model	Ranz–Marshall [37,38]
Evaporation model	Spalding [39]
Chemical mechanism	Pang et al. [40]
Turbulence-chemistry interaction	PaSR [41]
Turbulence sub-grid scale model	k-equation eddy viscosity model [42]

Table 3
Operating conditions of the reacting LES cases.

	T [K]	P [MPa]	O_2 [vol. %]	ϕ_m	IT [ms]
A	1000	4.29	0	0	0
B	1000	4.18	21	0	0
C	1000	4.16	20.15	0.3	0
D	1000	4.16	20.15	0.3	0.3
E	1000	4.16	20.15	0.3	0.6
F	1000	4.16	20.15	0.3	0.9
G	1000	4.16	20.15	0.3	1.2

2.2. Numerical schemes and models

In this study, Eqs. (1)–(4) are solved using OpenFOAM-4 [31] with a finite volume method and second-order accuracy schemes. Specifically, a filtered-linear scheme is adopted for spatial discretization of the convection and diffusion terms while an implicit backward scheme is employed for temporal integration. The chemical reactions are integrated using a finite-rate chemistry, in which a set of ordinary differential equations is solved using the linearly implicit Euler method [32]. The same schemes and methods have been used in the previous LES spray flame studies [22,33–35].

Table 2 shows the numerical methods and models adopted in the present LES. The liquid droplets of n-heptane fuel are injected as parcels into the domain at a number rate of 20 million per second and a mass flow rate of [43]. The drag coefficient C_D in Eq. (5) is set to 0.426 as suggested by Ref. [33]. The droplets primary and secondary break-up of are considered using a Rosin–Rammler size distribution and a hybrid Kelvin Helmholtz–Rayleigh Taylor (KH–RT) model [44]. The model constant B_1 is introduced to account for internal flow effects of the nozzle flow on the breakup time. B_1 and the droplet RT breakup diameter constant, C_{rt}, are set to 18 and 0.1 as suggested by Refs. [45,46]. The model constants n, d_{mean} and d_{max} in Rosin–Rammler distribution are set to 3, 50 μm and 100 μm, respectively. Those models and constants in the Lagrangian framework have been employed and validated in previous studies for spray modeling [14,36,47]. A k-equation eddy-viscosity model [42] with model constants $C_k = 0.07$ and $C_e = 0.3$ is used for the closure of LES SGS terms. This SGS model and the associated model constants are chosen based on the ECN LES in Refs. [33,34,48]. The current LPT configurations and SGS model are validated against the ECN non-reacting spray experiment. The model validation can be found in Section 4.1.

The partially-stirred reactor (PaSR) model [49] is coupled with a chemical mechanism to model $\widetilde{\dot{\omega}}_{Y_i}$ and $\widetilde{\dot{\omega}}_h$ in Eq. (3) and (4). PaSR has been widely applied in previous works on spray combustion [41,50,51]. In the PaSR model, the turbulence-chemistry interaction (TCI) is considered by including the Kolmogorov scale mixing in each computational cell [41]. Filtered reaction rates and heat release rate are calculated through a local coefficient $\kappa(x, y, z)$, e.g., $\widetilde{\dot{\omega}}_{Y_i} = \kappa\dot{\omega}_{Y_i}$ and $\widetilde{\dot{\omega}}_h = \kappa\dot{\omega}_h$. κ is proportional to the ratio of the chemical reaction time to the total conversion time in the reactor, i.e., $\kappa = \tau_c/(\tau_m + \tau_c)$. τ_c and τ_m are the local chemical reaction and micromixing time scales determined by [41]:

$$\frac{1}{\tau_c} = max\left\{\frac{-\dot{\omega}_f}{Y_f}, \frac{-\dot{\omega}_o}{Y_o}\right\}, \qquad \tau_m = C_{mix}\sqrt{\tau_k\tau_t}, \tag{6}$$

where subscripts f and o are the species indexes of fuel and oxidizer, respectively. τ_k and τ_t are Kolmogorov and Taylor time scales. C_{mix} is a model constant, which is set to 0.3 according to the previous LES spray flame [50].

A skeletal mechanism with 283 reactions and 68 species, originally developed by Lu et al. [52] and revised by Pang et al. [40] for Spray-H simulations, is selected for modeling chemical reactions and heat release. This mechanism was previously employed in direct numerical simulation of methanol fueled and n-heptane ignited DF combustion [53]. A methanol subset mechanism is present in this mechanism, which has shown good agreement with experiments [54] on the prediction of methanol IDT under engine-like conditions [35]. The chemistry coordinate mapping (CCM) approach [55,56] is used to speedup the integration of the chemical reactions, which consumes 95% of the CPU times in the present LES. The TCI model, chemical mechanism, CCM are validated using the experimental IDT and pressure rise profile in Section 4.1.

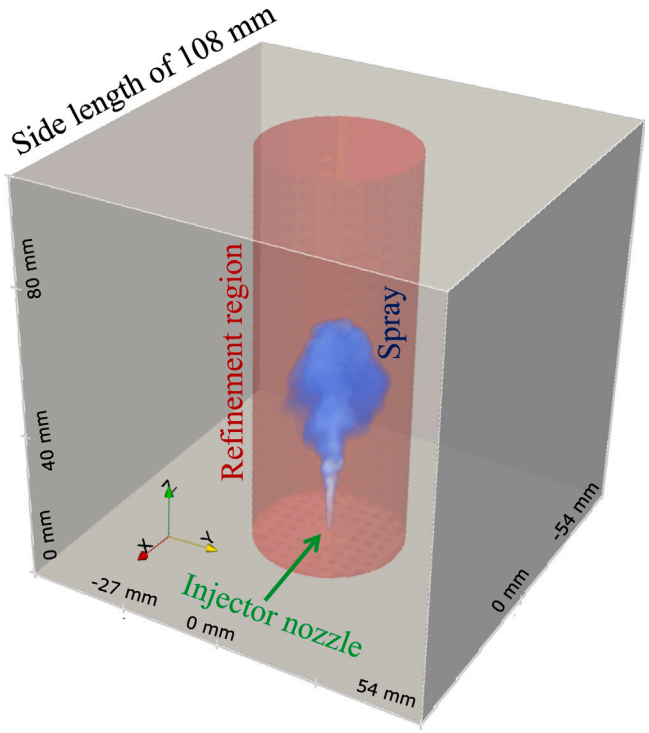

Fig. 1. The computational domain. The mesh refinement region is colored as red while the spray is colored as blue. Liquid fuel is initialized from the injector nozzle on the x-y plane. (For interpretation of the references to colour in this figure legend, the reader is referred to the web version of this article.)

3. Case specifications

Table 3 shows the LES cases and the corresponding operating conditions. All the cases have a cubical computational domain with each side length of 108 mm, which is the same size and shape as the ECN Spray-H experiments [29]. Fig. 1 shows the computational domain. Liquid n-heptane is injected from a nozzle into the domain and mixed with high temperature (1000 K) and high density (14.8 kg/m^3) ambient gas. The ambient gas is assumed to be quiescent and homogeneous, following the previous LES [14,33,34]. Cases A (non-reacting) and B (SF reacting) are chosen from Spray-H experiments for the model validation. The ambient gas compositions in Cases A and B are adopted from the experiments [29]. In Case A, the ambient gas is designed to be oxygen-free to solely investigate the n-heptane injection, atomization and evaporation at 1000 K. The ambient gas is a mixture of nitrogen

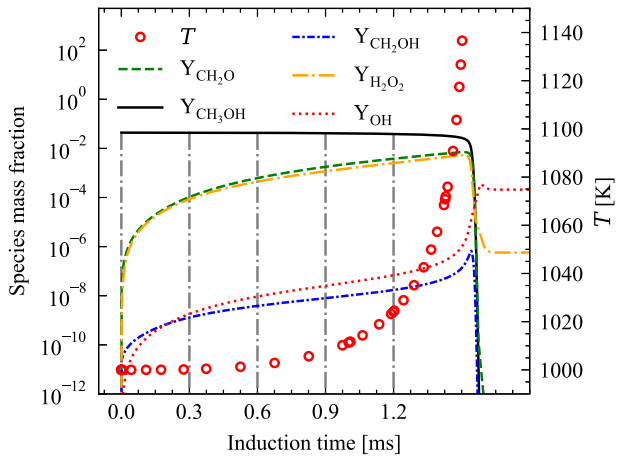

Fig. 2. Zero-dimensional simulation of homogeneous methanol/air mixture in a constant volume chamber. The initial condition is equivalence ratio of 0.3, initial temperature of 1000 K and pressure of 4.16 MPa. Auto-ignition is observed at 1.56 ms. Lines denote the main intermediate species mass fraction. Symbols are temperature. Five vertical lines represent the induction times from 0 to 1.2 ms.

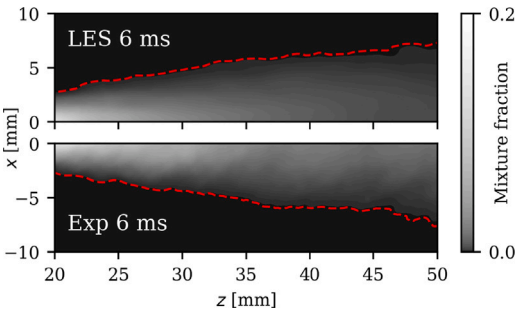

Fig. 3. Mixture fraction (Z) distribution (in x-z plane) from LES (upper) and experiments [29] (bottom) at 6 ms ASI. The dash line is an iso-contour of Z = 0.02. The experimental data is ensemble averaged from 30–40 experimental samples, while the LES data is time averaged from 2 ms to 6 ms ASI.

(N_2), water vapor (H_2O) and carbon dioxide (CO_2), with associated volumetric concentration of 89.71%, 3.77% and 6.52%, respectively. In Case B, the volumetric concentrations of oxygen (O_2), N_2, H_2O and CO_2 are 21%, 69.33%, 3.56% and 6.11%, respectively. This composition is set to mimic the pressurized preheated air in the naturally aspirated diesel engine. Following the workflow in the previous LES [14,15,18], the DF simulations are carried out upon the model validation in SF simulations, i.e., Cases A and B are firstly validated against ECN Spray-H experiments. In the DF cases (Cases C to G), the evaporated methanol is mixed with the air (the same compositions as the ambient air in Case B) to form a homogeneous mixture (CH_3OH 4.03%, O_2 20.15%, N_2 66.54 %, CO_2 5.86% and H_2O 3.42%, on volume basis). The concentration of methanol is characterized by the methanol/air equivalence ratio (ϕ_m). In the current LES of DF cases, ϕ_m is 0.3, which corresponds to the medium-load DF engine condition [57]. The initial temperature and pressure are comparable to the in-cylinder conditions of naturally aspirated DF engines near TDC.

In the current LES, the IT effects are considered by changing the SOI time. Case C serves as the DF baseline case, in which SOI is set at the beginning of the simulation, i.e., IT is 0 ms. Cases D to G are the control cases with IT from 0.3 to 1.2 ms. In the case where the SOI is retarded, the ambient methanol oxidation occurs for a longer period of time. In other words, the n-heptane is delivered into ambient methanol/air mixtures with different compositions. Before the start of injection, the ambient methanol/air is homogeneous and quiescent. The local temperature and species mass fractions are uniformly distributed in the domain, the PaSR local coefficient κ is equal to unity, independent of the location. In order to obtain the ambient compositions arisen from different IT, a zero-dimensional (0-D) simulation in a closed reactor with the current chemical mechanism is conducted prior to the LES. The initial condition of the 0-D simulation is set to those similar to the LES case (1000 K, 4.16 MPa, ϕ_m 0.3, and O_2 volume fraction of 20.15%). Fig. 2 shows the results of temperature and key intermediate species in this 0-D simulation. The ambient species mass fraction, temperature, and pressure in Cases C to G at their respective ITs are taken from this 0-D simulation results, instead of simulating the LES from the beginning to reduce the computational cost.

The liquid fuel n-heptane has a fuel temperature of 373 K. Following the setup in the Spray-H experiment [29], a total mass of 17.8 mg n-heptane is injected through a 100 μm diameter nozzle in 6.8 ms. The injection pressure inside the injector is fixed at 150 MPa, while the ambient pressure is about 4 MPa (varies in cases, cf. Table 3), leading to an initial droplet velocity of around 500 m/s.

4. Results and discussion

4.1. Model validation

Four sets of regular hexahedral meshes are used for grid sensitivity study. In these four meshes, a minimum grid size of 0.5, 0.375, 0.25, and 0.125 mm is performed in a local refinement region, with the total number 0.37, 0.89, 1.93 and 14.2 million computational cells, respectively. The flow time step depends on the maximum Courant–Friedrichs–Lewy (CFL) number, which is chosen as 0.1. A 0.1 ns initial time step of the chemical time step is adopted for chemical reaction integration. The temporal evolution of vapor penetration length (VPL) and liquid penetration length (LPL) for different grid sizes under the non-reacting conditions are shown in Appendix . The mesh sensitive analysis indicates that the 0.25 mm mesh provides reasonable mesh-insensitive results. This mesh is therefore adopted in the following simulations.

Fig. 3 shows the mixture fraction in the streamwise cross-section (x-z plane). Following suggestions in Ref. [22], the mixture fraction is calculated from a transport equation instead of using Bilger mixture fraction definition [58]. The experimental data [29] are measured by Rayleigh scattering. The LES results are obtained from non-reacting Case A. Fig. 4 shows temperature profiles at 20 and 25 mm downstream. It is worth noting that 30–40 samples at 6.0 ms ASI are extracted and ensemble averaged in experiments, while LES has only one realization. To obtain the averaged value in LES, a time average is performed in the non-reacting Case A, i.e., 400 instances with a time interval of 0.01 ms are used from 2 ms to 6 ms ASI. It is shown that a fairly good agreement of mixture fraction and non-reacting temperature distributions is achieved in the current LES, implying that the present mesh and models are able to replicate the spray, breakup and evaporation processes.

For the reacting case, the predicted and the measured pressure rise (the difference between the averaged pressure in the combustion chamber and its initial value) are shown in Fig. 5. It is well-known that, under engine conditions, n-heptane spray combustion has two-stage ignitions. In this study, the first stage ignition is indicated by the first peak of the temperature time derivative while the second stage ignition is indicated by the occurrence of the maximum temperature time derivative. IDTs are then defined as the time from SOI to the two-stage ignition events, denoted as τ_1 and τ_2. In the associated ECN experiment [29], τ_2 = 0.53 ms is measured. The corresponding IDT in the current LES of the reacting SF Case B is τ_2 = 0.50 ms. It is shown that the present LES is capable of replicating fairly well the pressure rise and IDT.

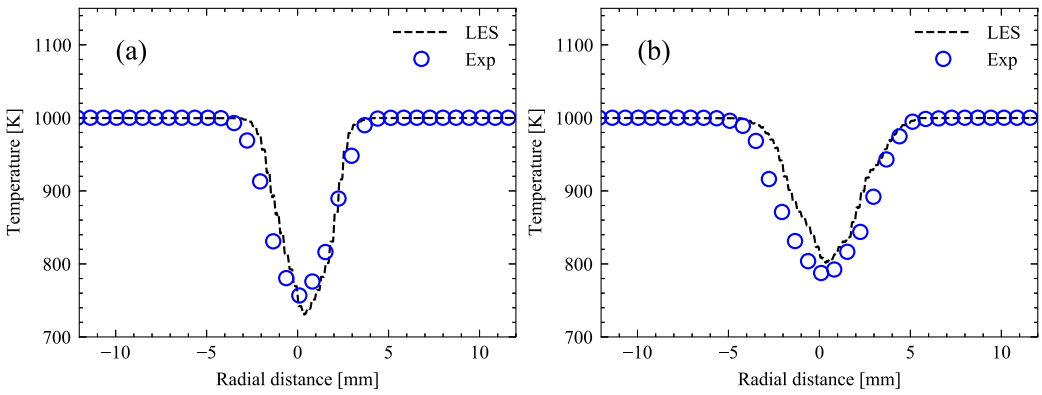

Fig. 4. The temperature radial profiles in non-reacting LES and corresponding experiments [29]. (a) 20 mm downstream, and (b) 25 mm downstream.

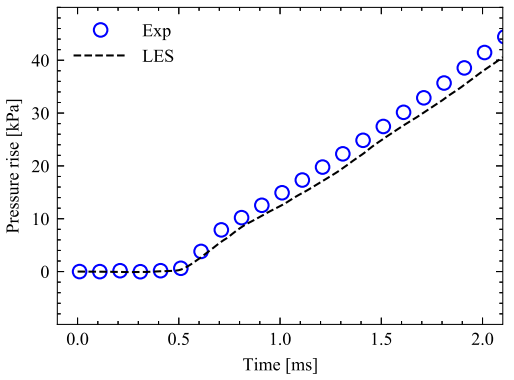

Fig. 5. Temporal evolution of the pressure rise in Case B and measurements [29].

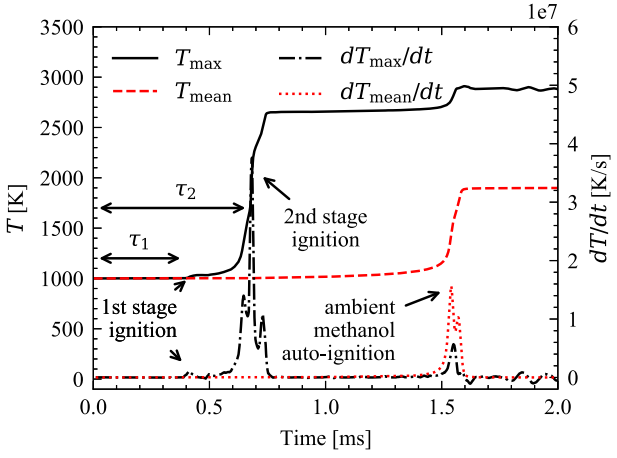

Fig. 6. Three stage ignitions in Case C characterized by T_{max}, T_{mean}, and their time derivative dT/dt.

4.2. The induction time effects on n-heptane and methanol IDT

In DF case, three-stage ignitions are found under current conditions. Following the definitions in SF case, the first and second stage IDTs, i.e., τ_1 and τ_2, in DF cases are observed and defined from the temporal evolution of the maximum temperature in the spray region. Apart from that, the third stage ignition is also observed. Fig. 6 shows the temporal evolution of T_{mean} and T_{max} in Case C. T_{mean} is the spatially averaged temperature while T_{max} is the maximum temperature in the spray region, i.e., mixture fraction $Z > 0.001$. In the present DF case setup, the total energy of n-heptane is much lower than methanol. The heat release from n-heptane is too weak to increase T_{mean} significantly, e.g., only 15.41 K increase of T_{mean} is observed in SF Case B at 2 ms. However, a rapid T_{mean} rise is observed after 1.5 ms, indicating the auto-ignition of methanol or the third stage ignition. The auto-ignition delay time of the ambient mixture is denoted as τ_{amb}, which is defined as the time at which the maximum time derivative of the ambient averaged temperature is achieved. Before the ambient methanol auto-ignition, the pressure in the constant volume chamber increases slowly. The n-heptane spray is under constant pressure combustion condition, the stoichiometric mixture of n-heptane/methanol–air has an adiabatic flame temperature of 2731 K. After τ_{amb}, ambient methanol is consumed under constant volume combustion condition. The average temperature and pressure in the constant volume chamber increase up to 1889 K and 8.02 MPa, respectively. In ambient methanol/air combustion products, residual oxygen has a mass fraction of 0.152. The n-heptane spray is continuously supplied and mixed with high-temperature and high-pressure oxygen and forms a new stoichiometric mixture, which has an adiabatic flame temperature of 2871 K. Therefore, an increase of T_{max} is observed after τ_{amb}.

Fig. 7 shows τ_1, τ_2 and τ_{amb} in DF Cases C to G. In terms of the n-heptane spray ignition, both the first and the second stage IDTs decrease with the increase of the IT. For example, τ_1 decreases from 0.414 ms (in 0 ms IT case) to 0.380 ms (in 0.3 ms IT case). No τ_1 data is available for the 1.2 ms IT case, since two-stage heat release is absent in Case G. τ_2 decreases continuously from 0 ms IT to 0.9 ms IT. A further decline of τ_2 is observed in the 1.2 ms IT case, in which the auto-ignition of the ambient mixture (0.357 ms ASI) is slightly ahead of the spray second stage ignition (0.366 ms ASI) in the 1.2 ms IT case. In other words, n-heptane spray is ignited by the ambient mixture. In general, the impact of IT on the spray IDTs is evident, a longer IT leads to shorter τ_1 and τ_2. On the other hand, τ_{amb} is shortened in DF spray combustion. In the 0-D simulation, cf. Fig. 2, $\tau_{amb} = 1.560$ ms. As shown in Fig. 5, the pressure rise in Case B is 25.35 kPa at 1.560 ms ASI. A 0-D simulation in such a elevated pressure condition results in a τ_{amb} of 1.550 ms, i.e., the pressure rise induced from the spray combustion contributes to the reduction of τ_{amb}. In the DF mode, τ_{amb} is 1.540 ms in Case C and 1.557 ms in Case G, respectively. τ_{amb} increases with the increase of IT, however, only a minor τ_{amb} increase is observed under the present condition.

Fig. 8 shows temporal evolution of HRR in the ambient mixture and the spray region. The volumetric integration of the chemical HRR ($\dot{Q}$) is performed in the whole computational domain (V_{tot}) and in the spray region (computational cells with a mixture fraction of $Z \geq 0.001$, denoted as V_{spray}). $\dot{Q}_{tot}$ and $\dot{Q}_{spray}$ are the volumetric integration of $\dot{Q}$ within V_{tot} and V_{spray}, i.e., $\dot{Q}_{tot} = \int_{V_{tot}} \dot{Q} dV$ and $\dot{Q}_{spray} = \int_{V_{spray}} \dot{Q} dV$. $\dot{Q}_{amb}$ is the volumetric integration of the chemical HRR in the ambient mixture, $\dot{Q}_{amb} = \dot{Q}_{tot} - \dot{Q}_{spray}$. It is observed that the heat source is mainly from the ambient mixture $\dot{Q}_{amb}$. The maximum ratio $\dot{Q}_{spray}/\dot{Q}_{amb}$ is found at around 1.0 ms in Case C. This ratio is

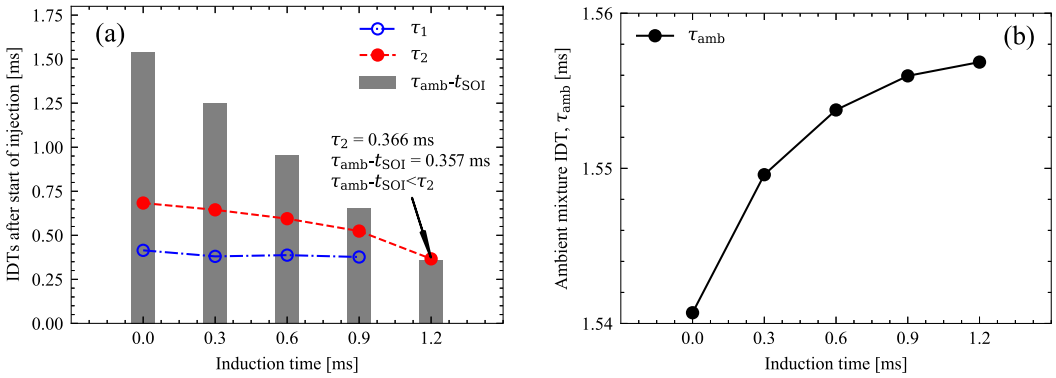

Fig. 7. (a) τ_1 and τ_2, (b) τ_{amb} in DF Cases C to G. Bars in (a) represent τ_{amb}-t_{SOI}, where t_{SOI} is the start of injection time.

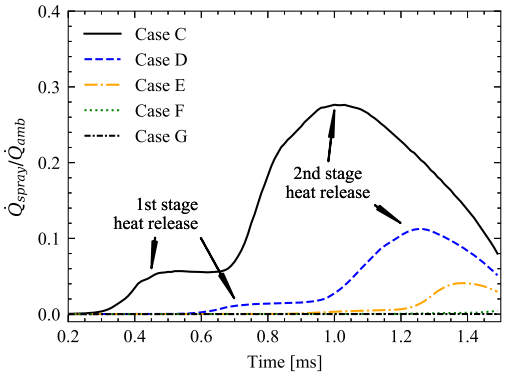

Fig. 8. The ratio of spatially integrated chemical HRR in the spray region and ambient mixture region, $\dot{Q}_{spray}/\dot{Q}_{amb}$.

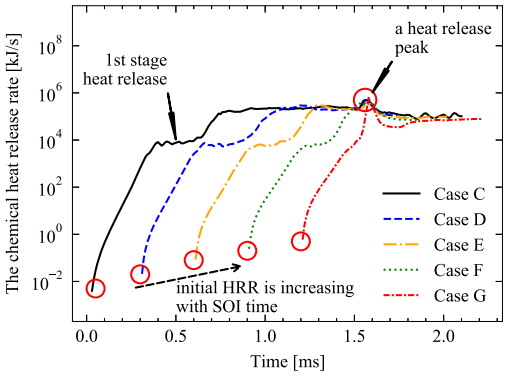

Fig. 9. The spatially integrated chemical HRR from the n-heptane spray region.

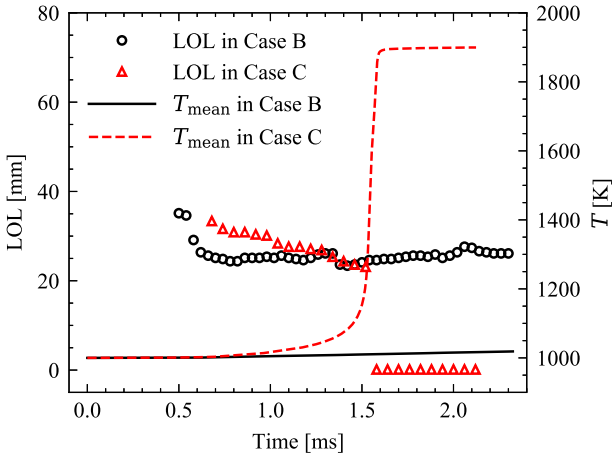

Fig. 10. Temporal evolution of LOL and T_{mean} in Case B and C.

remarkably decreased from IT 0 to 1.2 ms, e.g., a maximum ratio of 0.276 in Case C, 0.113 in Case D, and 0.0002 in Case F. This HRR ratio changes imply the increase of τ_{amb} in large IT cases, while the minor contribution of $\dot{Q}_{spray}$ to $\dot{Q}_{tot}$ explains the negligible effects of n-heptane on τ_{amb}.

Fig. 9 shows $\dot{Q}_{spray}$, i.e., volumetric integration of the chemical HRR in the spray region, in a logarithmic scale. In Cases C, D, E and F, it is observed that HRR undergoes two stage growth, attributed to the heat release associated with the two stage ignitions. In Case C, the first and second stage heat releases are indicated as two plateaus. The two plateaus start shortly after the first (τ_1 = 0.41 ms) and second (τ_2 = 0.68 ms) stage ignitions, respectively. From Case C to F, IT increases while the transition time of the two plateaus decreases. It is also seen that the initial HRR increases with the increase of IT. This implies that a late start of injection yields an earlier heat release and a short transition period of n-heptane two stage heat release. It is found that both plateaus disappear in Case G, while a $\dot{Q}_{spray}$ peak is observed around τ_{amb}. This peak is a unique phenomenon for DF spray cases. The same peak is also observed in Cases D to F but not in Case B. The surrounding ambient methanol ignition triggered the final ignition of the spray region. A similar observation is found in Fig. 6, where a peak of dT_{max}/dt and dT_{mean}/dt appears simultaneously, associated with an increase of T_{max} and T_{mean}.

Fig. 10 shows the evolution of the flame lift-off length (LOL) and T_{mean} in Cases B and C. LOL is calculated as the nearest axial distance from the injector to the flame front, which is indicated by iso-contour of OH species equal to 0.0001. The experimental LOL in SF case is 17 mm under the present condition [29]. In Case B, LOL starts after the second stage ignition τ_2 = 0.5 ms and oscillates between 20 mm and 30 mm, while T_{mean} increases slowly and continually. In Case C, LOL starts after 0.68 ms and decreases slowly until 1.55 ms, at which the ambient mixture is ignited as T_{mean} increases significantly. A high T_{mean} triggers the high temperature chemistry of unburned n-heptane near the nozzle, thus the flame front is observed near the nozzle accompanied by a relative high HRR, i.e., the peak in Fig. 9.

4.3. The induction time effects on the flame structures

Fig. 11 shows the axial distribution of species mass fractions and temperature in DF cases. Three columns represent 0.3 ms, 0.6 ms and 0.9 ms instantaneous states after the start of injection (ASI). A vertical line is plotted in each sub-figure to show the n-heptane vapor penetration lengths, which are 26 mm, 38 mm and 47 mm from left to right. Note that the n-heptane vapor penetration lengths are extracted

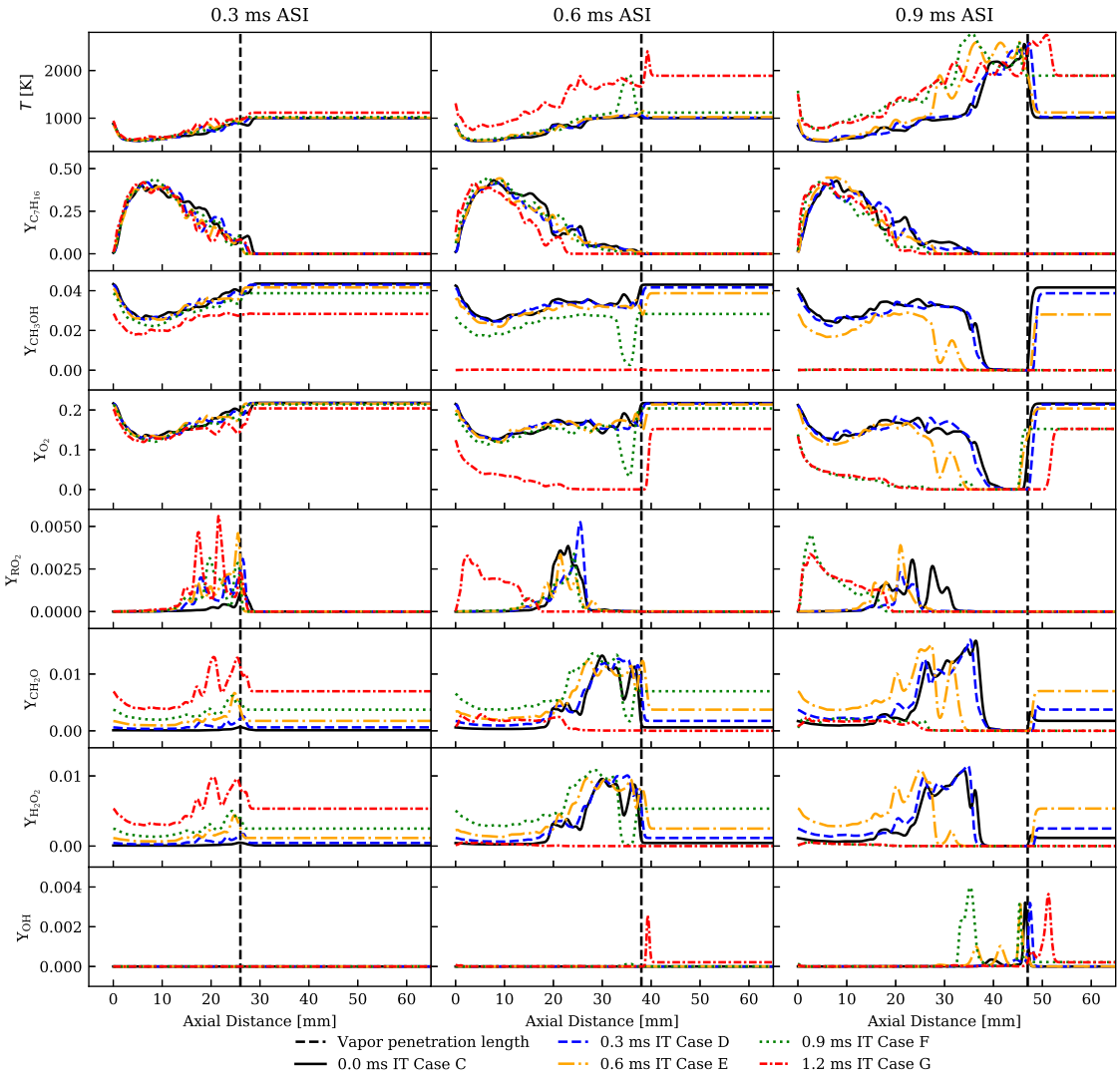

Fig. 11. The axial distribution of species mass fractions and temperature for DF Cases C to G.

from the non-reacting case, which has a slower penetration speed compared to reacting cases. Thus, the vertical line is only indicative but not exact. In the region of an axial distance larger than the vapor penetration length, to which n-heptane vapor has yet reached, a nearly homogeneous methanol/air mixture and its reaction products are found. In the region of an axial distance smaller than the vapor penetration length, i.e., left hand side of the vertical line, n-heptane vapor is mixed with ambient methanol. For brevity, the left and right domains are hereinafter named as spray interaction region and ambient methanol region. In the spray interaction region, liquid n-heptane evaporates and mixes with the ambient mixture. The temperature in this region decreases due to the spray evaporation and mixing of the low temperature n-heptane. The local CH_3OH and O_2 mass fractions are lower than those in the ambient methanol region at 0.3 ms ASI. On the other hand, the ambient CH_3OH and O_2 mass fractions decrease while temperature increases with the increase of IT, e.g., the ambient temperature in Case G (1.2 ms IT) is higher than in Case C (0 ms IT) at 0.3 ms ASI. This is an indicator of the auto-ignition reactions in the ambient methanol region. At 0.6 and 0.9 ms ASI, CH_3OH and O_2 mass fractions are further consumed and give rise to an obvious temperature increase. For instance, over 1800 K temperature and zero mass-fractions of CH_3OH are observed in Case G at 0.6 ms and Case F at 0.9 ms ASI. This obvious temperature increase and CH_3OH consumption indicate an auto-ignition of the ambient methanol.

In a n-heptane SF spray flame, an increase of heptyl-peroxide (RO_2) denotes the first stage ignition [29]. After the first stage ignition, RO_2 is consumed in low temperature reactions and generates subsequently intermediate species such as formaldehyde, CH_2O, which may be used as a marker of cool flame [18]. In further downstream, CH_2O is consumed in high temperature chemistry (HTC) following the formation of hydroxyl radicals (OH). The emergence of OH indicates the second stage ignition and a high temperature flame. In the high temperature flame, CH_2O is oxidized to form CO, CO_2 and H_2O.

In then n-heptane/methanol DF spray flame, cool flame and high temperature flame are also established after the first and second stage ignitions of n-heptane spray, respectively. In reality, the premixed flame is initialized after the second stage ignition. However, numerical simulation of the premixed flame under the present high temperature and high pressure conditions is challenge. In the present study, the premixed flame is not modeled as the ignition event is in focus. Before auto-ignition of the ambient mixture, both cool flame and high temperature flame are observed. For example, at 0.3 ms ASI, RO_2 and CH_2O appear in all cases, indicating that a cool flame is established. The difference is that the RO_2 mass fraction is higher in the retarded SOI time cases. This difference is rather notable in CH_2O mass fraction. In addition, in all cases, a plateau of CH_2O mass fraction is observed in the ambient mixture, i.e., on the right side of the vertical line. As suggested in Ref. [35], this CH_2O is attributed to reactions of CH_2OH +

$O_2 = CH_2O + HO_2$ and $CH_3O + O_2 = CH_2O + HO_2$. After auto-ignition of the ambient mixture, high temperature flame still exists while cool flame disappears. For example, from 0.6 to 0.9 ms ASI in Case F, CH_2O mass fraction drops dramatically while RO_2 is formed upstream. At 0.9 ms ASI, high temperature flame and HTC are observed upstream in Case G and Case F characterized by the oxidation of CH_2O. The observation of the upstream high temperature flame is consistent with swift changes of flame lift-off in Fig. 10.

4.3.1. The cool flame

As an indicator of the cool flame, CH_2O is used to study the evolution of the cool flame. Fig. 12 shows the temporal evolution of the averaged CH_2O mass fraction for a given range of axial locations z, so-called intensity-axial distance-time (IXT) plots. The blue color in subplots Fig. 12a and b represents the averaged CH_2O mass fraction in the whole domain. At each time step, the CH_2O mass fraction is averaged in the cross-flow (x-y) plane, i.e., $\overline{Y}_{CH_2O}(z,t) = \iint Y_{CH_2O}(x,y,z,t)dxdy \,/\, \iint dxdy$. The blue color in subplot Fig. 12c shows the averaged CH_2O mass fraction in the spray region, i.e., $\overline{Y}_{s,CH_2O}(z,t) = \iint H(x,y,z,t)Y_{CH_2O}(x,y,z,t)dxdy \,/\, \iint dxdy$. H is a step function, $H = 1$ when local mixture fraction $Z > 0.001$, $H = 0$ when $Z < 0.001$. In Fig. 12a, CH_2O appears after the first stage ignition τ_1 at around 20 mm, indicating the onset of the cool flame. The formation of this cool flame is found downstream, around 35 mm at the second stage ignition τ_2. Thereafter, the downstream CH_2O is consumed immediately in the high temperature reactions (HTC), e.g. $CH_2O + OH = HCO + H_2O$. Hence, an isolated region can be found in Fig. 12a, denoted by a red circle. Finally, the cool flame is stabilized in the SF spray flame.

In Fig. 12b and c, the onset of the cool flame in DF case occurs further downstream at around 25 mm. Since CH_2O is also formed in the auto-ignition reactions of the ambient methanol, CH_2O is subsequently observed both downstream and upstream and its mass fraction increases with time. As shown in Fig. 10, the flame LOL decreases once the high temperature flame is established at τ_2. The consumption of CH_2O occurs both downstream and upstream in HTC, shown as a wedge-shape region after 0.7 ms in Fig. 12b. Fig. 12c shows the averaged CH_2O in spray region, where cool flame is not stabilized. After 0.7 ms, downstream CH_2O in the spray region is also consumed, while a formation of CH_2O is found upstream. Furthermore, an absence of CH_2O is observed after ambient methanol auto-ignition. The wedge-shape region after τ_2 and elimination of CH_2O after τ_{amb} imply that the cool flame in DF spray combustion will not be stabilized.

4.3.2. The high temperature flame

In order to analyze the IT effects on high temperature ignition kernel formation, a key HTC species, hydrogen peroxide (H_2O_2), is selected and analyzed in detail. H_2O_2 is important due to reaction $H_2O_2 + M = OH + OH + M$ (denoted as R1). R1 is a chain branching reaction giving rise to OH formation and high temperature ignition. Following the recommendation of Refs. [14,59], the HTC and high temperature ignition kernel formation in spray flame is identified with a consumption of H_2O_2.

Fig. 13 shows snapshots of the streamwise (in x-z plane) species mass fraction, including H_2O_2, OH and CO, distribution in DF cases. An early formation of H_2O_2 is firstly found on $Z > Z_{st}$, i.e., fuel-rich side, and then found on fuel-lean side in short IT cases (Cases C, D and E). However, in longer IT cases (Cases F and G), the maximum H_2O_2 mass fraction is observed on $Z < Z_{st}$, i.e., fuel-lean side, due to the H_2O_2 formation in ambient methanol auto-ignition reactions. As shown in Fig. 2, the ambient H_2O_2 mass fraction in the long IT is significantly higher than that in the short IT instance. High H_2O_2 concentration promotes the high temperature ignition kernel formation. As a consequence, an earlier formation of high temperature flame is observed in Cases F and G.

As discussed in Fig. 7, τ_{amb}-t_{SOI} in Cases E, F and G are 0.953, 0.656 and 0.357 ms, respectively. The ambient methanol auto-ignition

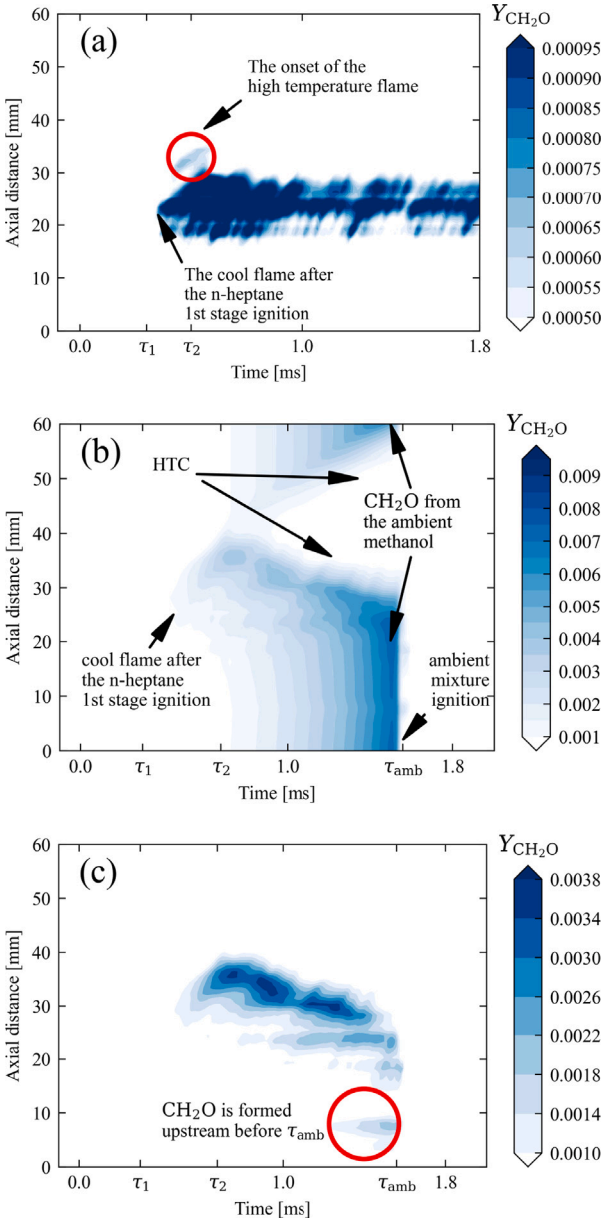

Fig. 12. IXT plots of cool flame evolution in SF Case B (a), DF Case C (b) and (c). The blue color in (a) and (b) shows the averaged CH_2O mass fraction in the whole domain, $\overline{Y}_{CH_2O}(z,t)$. The blue color in (c) represents the averaged CH_2O mass fraction in the spray region, $\overline{Y}_{s,CH_2O}(z,t)$. (For interpretation of the references to colour in this figure legend, the reader is referred to the web version of this article.)

and flame structure after τ_{amb} are also shown in Fig. 13. After τ_{amb}, H_2O_2 in fuel-lean mixture is consumed and a low mass fraction ($Y_{OH} \approx 0.0002$, not visible on present scale) of OH is produced. Shortly after ambient mixture auto-ignition, the remaining H_2O_2 is found in fuel-rich mixture in Case G at 0.4 ms ASI. The similar observation is found in Case E at 1.0 ms. In fuel-rich region, the evaporation of the liquid n-heptane results in a local low temperature zone, which slows down the H_2O_2 consumption reaction R1. In all DF cases, CO is formed in fuel-rich and high-temperature regions ($Z > Z_{st}$, T>2000 K). OH is found in the lean mixture region (Z<Z_{st}) in all the DF cases, enveloped by stoichiometric mixture line and iso-line of T = 2000 K. Due to the methanol auto-ignition, the ambient temperature increases while oxygen concentration significantly reduces. A higher temperature leads to a higher OH production. A low oxygen concentration leads to

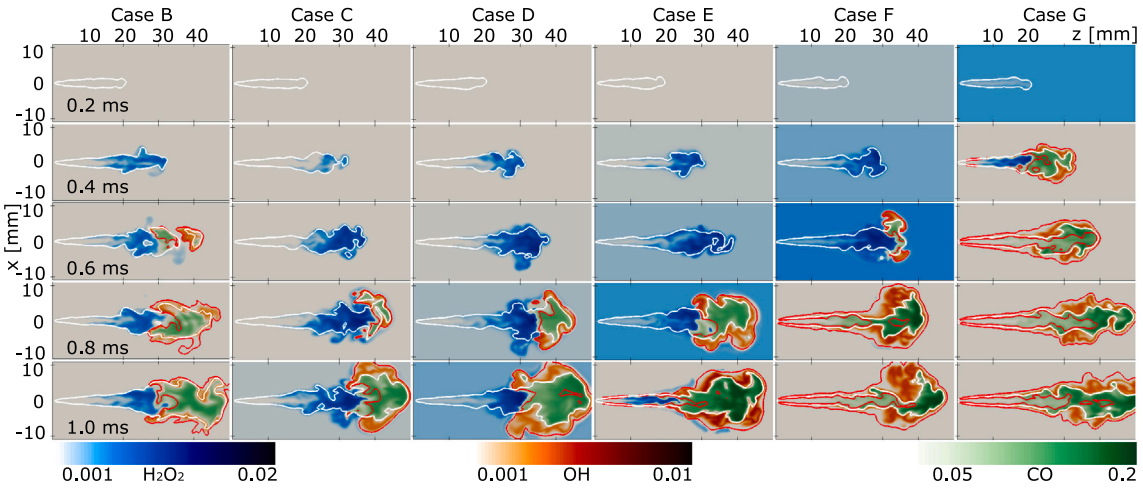

Fig. 13. The streamwise snapshots of species H_2O_2, OH and CO at 0.2–1.0 ms ASI (0.2 ms time interval from top to bottom) in DF Cases C to G (from left to right). Mass fractions smaller than a threshold are truncated to avoid overlaps, e.g., a threshold of 0.001 for OH and H_2O_2, 0.05 for CO. The white and red iso-lines represent stoichiometric mixture and temperature of 2000 K. (For interpretation of the references to colour in this figure legend, the reader is referred to the web version of this article.)

incomplete combustion and thus higher CO mass fraction. As a result, an increase of OH and CO mass fractions is also observed after τ_{amb}.

5. Conclusion

In dual-fuel (DF) engines, the primary fuel and pilot fuel are delivered separately. During the time interval, the ignition reactions in the primary fuel–air mixture take place and produce intermediate species, which interact with pilot fuel injection. Thus, the pilot fuel injection timing has a significant impact on the DF ignition and combustion. This impact is more severe for methanol-fueled DF engines. In this study, large-eddy simulations (LES) are performed to investigate the injection timing effects on the n-heptane/methanol DF combustion.

The studied DF combustion configuration is based on the Engine Combustion Network (ECN) constant volume chamber. Firstly, a mesh sensitive analysis is performed under experimental conditions of ECN Spray-H with four sets of meshes. Secondly, a non-reacting and a ECN Spray-H reacting case are extensively validated against the Spray-H experiments. The present LES model is shown to predict fairly well measured liquid and vapor penetration lengths, mixture fraction and temperature distributions, pressure rise and ignition delay times.

Five DF reacting cases are then defined and simulated to investigate the injection timing effects on DF combustion by varying the ignition induction time (IT), which is the time between the initial time of the ambient mixture and the start of n-heptane injection (SOI), from 0 to 1.2 ms. The primary fuel methanol is premixed with air in a constant volume chamber to form a homogeneous and quiescent mixture (T = 1000 K, ρ = 14.8 kg/m^3, equivalence ratio of 0.3). Liquid fuel n-heptane is injected into the chamber to mimic the pilot fuel in DF engines. The main findings on ignition, cool flame and high-temperature flame structures in n-heptane/methanol DF combustion are:

1. Three-stage heat releases are found in the DF spray combustion, including a) a weak heat release from the n-heptane first stage ignition at τ_1, b) a strong heat release from n-heptane second stage ignition at τ_2, and c) ambient methanol auto-ignition at τ_{amb}. τ_1 and τ_2 decrease with the increase of IT, while τ_{amb} increases with the increase of IT. This understanding is beneficial to a precise control of combustion phasing and heat release in DF engine.
2. Before τ_{amb}, the axial mass fractions of heptyl-peroxide (RO_2) and formaldehyde (CH_2O) are higher in the retarded SOI cases. After τ_{amb}, RO_2 is found near the injector nozzle, while CH_2O is eliminated, indicating that the cool flame disappears after the auto-ignition of the ambient methanol.
3. In the delayed SOI cases, an early formation of the high-temperature ignition kernel is observed. This is due to the higher mass fraction of hydrogen peroxide (H_2O_2) generated in the DF ambient mixture, which leads to hydroxyl radicals (OH) formation through the reaction H_2O_2 + M = OH + OH + M. In addition, OH is found in the lean mixture region ($Z<Z_{st}$) in all the DF cases.
4. After τ_{amb}, the unburned n-heptane near the injector nozzle is ignited, leading to a relative high heat release rate. A delayed SOI timing results in a shorter liftoff length and a larger high temperature region.

CRediT authorship contribution statement

Shijie Xu: Conceptualization, Investigation, Writing – original draft. **Shenghui Zhong:** Software, Investigation. **Ahmad Hadadpour:** Investigation, Validation. **Yan Zhang:** Software, Validation. **Kar Mun Pang:** Investigation, Writing – review & editing. **Mehdi Jangi:** Methodology. **Hesameddin Fatehi:** Supervision, Writing – review & editing. **Xue-Song Bai:** Supervision, Project administration, Funding acquisition, Writing – review & editing.

Declaration of competing interest

The authors declare that they have no known competing financial interests or personal relationships that could have appeared to influence the work reported in this paper.

Acknowledgments

This work was sponsored by the Swedish Research Council (VR), and Swedish Energy Agency through CECOST and KCFP. Shijie Xu was sponsored by China Scholarship Council. The simulations were performed on resources provided by the Swedish National Infrastructure for Computing (SNIC) at NSC, HPC2N and PDC.

Appendix. Mesh sensitivity

Fig. A.1 shows the four meshes with minimum grid size of 0.5, 0.25, 0.375 and 0.125 mm. A local refinement is used in all mesh configurations. For example, a 4 mm diameter (d) 12 mm height (h) cylinder, a connecting cone and a d = 20 mm h = 84 mm coaxial cylinder are adopted as the inner region in the mesh with 0.125 mm grid. Four coaxial cylinders (d_1, d_2, d_3 and d_4 are 4, 10, 14 and 20 mm,

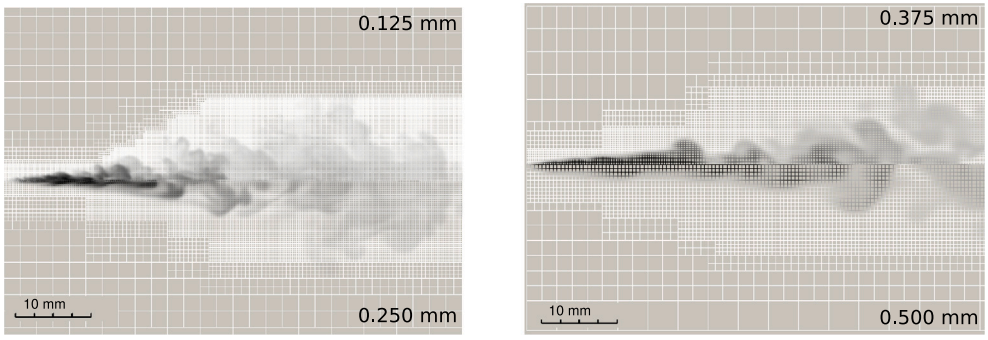

Fig. A.1. The streamwise snapshots of mixture fraction distribution at 1.5 ms ASI and mesh configuration with grid size of 0.125 and 0.25 (left), 0.375 and 0.5 mm (right).

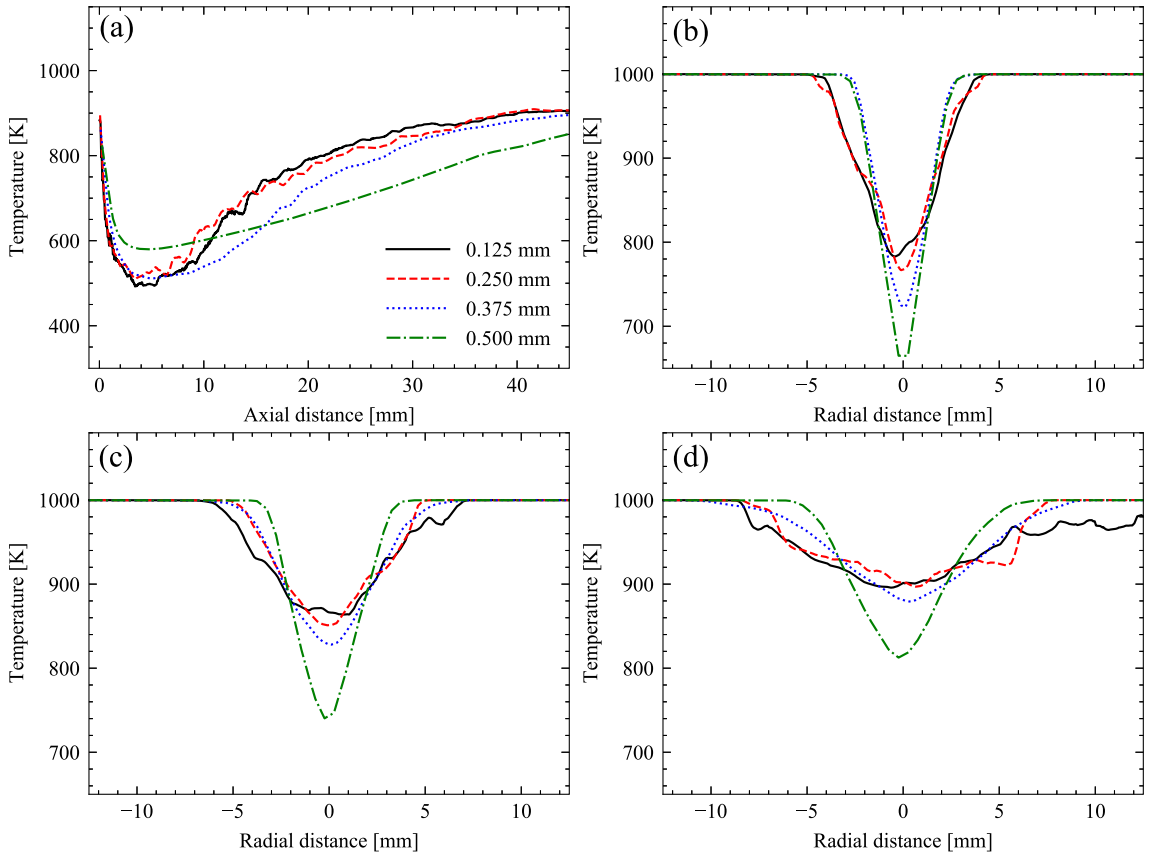

Fig. A.2. Time-averaged temperature (a) axial profiles, and radial profiles at (b) 20 mm, (c) 30 mm, and (d) 40 mm downstream, with grid size from 0.125 to 0.5 mm.

while h_1, h_2, h_3 and h_4 are 10, 10, 15 and 83 mm, respectively) constitute the inner region in meshes with 0.25, 0.375 and 0.5 mm grid. Fig. A.1 also shows the streamwise mixture fraction distribution at 1.5 ms ASI. The spray is captured in the inner region, in which the grid size is uniform.

Fig. A.2 shows the temperature axial and radial distributions in non-reacting LES Case A with different grid size. To avoid turbulent fluctuations, a time average is performed from 1.0 to 1.5 ms ASI. In all cases, temperature falls to 500 K in the liquid region upstream due to the heat absorption during n-heptane evaporation. A temperature increase is then observed downstream where n-heptane is mixed with high temperature methanol/air mixture. As compared to the finest mesh, a lower temperature in the mixing region and a higher temperature in the liquid region are predicted in coarse meshes, i.e., grid size of 0.5 and 0.375 ms. An insensitive result is obtained in mesh with 0.25 mm grid.

Fig. A.3 shows temporal evolution of LPL and VPL for non-reacting LES Case A and experiments [29]. LPL from the numerical simulations is axial distance from the nozzle to downstream location where 95% liquid fuel mass is evaporated. VPL is defined as farthest axial distance from the nozzle to iso-contour of a 0.1% mixture fraction [29]. As compared to the finest mesh, an underprediction of LPL and an overprediction of LPL are observed in the 0.5 mm grid coarse mesh. After 0.8 ms ASI, 0.375 mm grid mesh also results in a higher VPL. In terms of LPL and VPL, an insensitive result is obtained in mesh with 0.25 mm grid. This mesh was also used in several previous works [22,35,48,50,60]. As compared with measurements, the maximum error of VPL is only 2% in the 0.25 mm mesh.

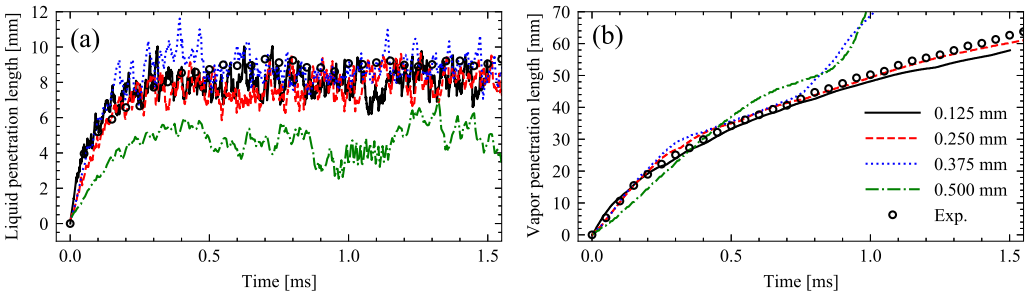

Fig. A.3. (a) the LPL, and (b) the VPL for non-reacting LES with grid size from 0.125 to 0.5 mm and experiments.

References

[1] Chmielniak T, Sciazko M. Co-gasification of biomass and coal for methanol synthesis. Appl Energy 2003;74(3–4):393–403.

[2] Olah GA. Beyond oil and gas: the methanol economy. Angew Chem Int Ed Engl 2005;44(18):2636–9.

[3] Verhelst S, Turner JW, Sileghem L, Vancoillie J. Methanol as a fuel for internal combustion engines. Prog Energy Combust Sci 2019;70:43–88.

[4] Tutak W, Lukacs K, Szwaja S, Bereczky A. Alcohol–diesel fuel combustion in the compression ignition engine. Fuel 2015;154:196–206.

[5] Li Y, Jia M, Liu Y, Xie M. Numerical study on the combustion and emission characteristics of a methanol/diesel reactivity controlled compression ignition (RCCI) engine. Appl Energy 2013;106:184–97.

[6] Wu T, Yao A, Yao C, Pan W, Wei H, Chen C, et al. Effect of diesel late-injection on combustion and emissions characteristics of diesel/methanol dual fuel engine. Fuel 2018;233:317–27.

[7] Li Y, Jia M, Xu L, Bai X-S. Multiple-objective optimization of methanol/diesel dual-fuel engine at low loads: A comparison of reactivity controlled compression ignition (RCCI) and direct dual fuel stratification (DDFS) strategies. Fuel 2020;262:116673.

[8] Duraisamy G, Rangasamy M, Govindan N. A comparative study on methanol/diesel and methanol/PODE dual fuel RCCI combustion in an automotive diesel engine. Renew Energy 2020;145:542–56.

[9] Kokjohn SL. Reactivity controlled compression ignition (RCCI) combustion. (Ph.D. thesis), The University of Wisconsin-Madison; 2012.

[10] Nazemi M, Shahbakhti M. Modeling and analysis of fuel injection parameters for combustion and performance of an RCCI engine. Appl Energy 2016;165:135–50.

[11] Srna A, von Rotz B, Herrmann K, Boulouchos K, Bruneaux G. Experimental investigation of pilot-fuel combustion in dual-fuel engines, part 1: Thermodynamic analysis of combustion phenomena. Fuel 2019;255:115642.

[12] Srna A, von Rotz B, Bolla M, Wright YM, Herrmann K, Boulouchos K, et al. Experimental investigation of pilot-fuel combustion in dual-fuel engines, part 2: Understanding the underlying mechanisms by means of optical diagnostics. Fuel 2019;255:115766.

[13] Schlatter S, Schneider B, Wright YM, Boulouchos K. N-heptane micro pilot assisted methane combustion in a rapid compression expansion machine. Fuel 2016;179:339–52.

[14] Kahila H, Wehrfritz A, Kaario O, Vuorinen V. Large-eddy simulation of dual-fuel ignition: Diesel spray injection into a lean methane-air mixture. Combust Flame 2019;199:131–51.

[15] Kahila H, Kaario O, Ahmad Z, Masouleh MG, Tekgül B, Larmi M, et al. A large-eddy simulation study on the influence of diesel pilot spray quantity on methane-air flame initiation. Combust Flame 2019;206:506–21.

[16] Tekgül B, Kahila H, Kaario O, Vuorinen V. Large-eddy simulation of dual-fuel spray ignition at different ambient temperatures. Combust Flame 2020;215:51–65.

[17] Karimkashi S, Kahila H, Kaario O, Larmi M, Vuorinen V. Numerical study on tri-fuel combustion: ignition properties of hydrogen-enriched methane-diesel and methanol-diesel mixtures. Int J Hydrogen Energy 2020;45(7):4946–62.

[18] Wei H, Zhao W, Qi J, Liu Z, Zhou L. Effect of injection timing on the ignition process of n-heptane spray flame in a methane/air environment. Fuel 2019;245:345–59.

[19] Yousefi A, Birouk M, Lawler B, Gharehghani A. Performance and emissions of a dual-fuel pilot diesel ignition engine operating on various premixed fuels. Energy Convers Manage 2015;106:322–36.

[20] Zang R, Yao C, Yin Z, Geng P, Hu J, Wu T. Mechanistic study of ignition characteristics of diesel/methanol and diesel/methane dual fuel engine. Energy & Fuels 2016;30(10):8630–7.

[21] Gadalla M, Kannan J, Tekgül B, Karimkashi S, Kaario O, Vuorinen V. Large-eddy simulation of tri-fuel combustion: Diesel spray assisted ignition of methanol-hydrogen blends. Int J Hydrogen Energy 2021.

[22] Xu S, Zhong S, Pang KM, Yu S, Jangi M, Bai X-S. Effects of ambient methanol on pollutants formation in dual-fuel spray combustion at varying ambient temperatures: A large-eddy simulation. Appl Energy 2020;279:115774.

[23] McAllister S, Chen J-Y, Fernandez-Pello AC. Fundamentals of combustion processes. Vol. 302. Springer; 2011.

[24] NIST Chemistry WebBook. 2021, https://webbook.nist.gov/. (Accessed Sep 2021).

[25] Reitz RD, Duraisamy G. Review of high efficiency and clean reactivity controlled compression ignition (RCCI) combustion in internal combustion engines. Prog Energy Combust Sci 2015;46:12–71.

[26] Wang Q, Yao C, Dou Z, Wang B, Wu T. Effect of intake pre-heating and injection timing on combustion and emission characteristics of a methanol fumigated diesel engine at part load. Fuel 2015;159:796–802.

[27] Chen Z, Wang L, Zhang Q, Zhang X, Yang B, Zeng K. Effects of spark timing and methanol addition on combustion characteristics and emissions of dual-fuel engine fuelled with natural gas and methanol under lean-burn condition. Energy Convers Manage 2019;181:519–27.

[28] Gharehghani A. Load limits of an HCCI engine fueled with natural gas, ethanol, and methanol. Fuel 2019;239:1001–14.

[29] Sandia National Laboratories. Engine combustion network. 2019, https://ecn.sandia.gov. (Accessed Jan 2021).

[30] Gong C. Numerical studies of turbulent combustion under diesel engine related conditions. (Ph.D. thesis), Lund University; 2016.

[31] Weller HG, Tabor G, Jasak H, Fureby C. A tensorial approach to computational continuum mechanics using object-oriented techniques. Comput Phys 1998;12(6):620.

[32] Wanner G, Hairer E. Solving ordinary differential equations II. Springer Berlin Heidelberg; 1996.

[33] Gong C, Jangi M, Bai X-S. Large eddy simulation of n-dodecane spray combustion in a high pressure combustion vessel. Appl Energy 2014;136:373–81.

[34] Gong C, Jangi M, Lucchini T, D'Errico G, Bai X-S. Large eddy simulation of air entrainment and mixing in reacting and non-reacting diesel sprays. Flow Turbul Combust 2014;93(3):385–404.

[35] Xu S, Pang KM, Li Y, Hadadpour A, Yu S, Zhong S, Jangi M, et al. LES/TPDF investigation of the effects of ambient methanol concentration on pilot fuel ignition characteristics and reaction front structures. Fuel 2020;119502.

[36] Beale JC, Reitz RD. Modeling spray atomization with the kelvin-Helmholtz/Rayleigh-taylor hybrid model. Atomization Sprays 1999;9(6):623–50.

[37] Ranz WE, Marshall WR. Evaporation from drops, part i. Chem Eng Prog 1952;48(3):141–6.

[38] Ranz WE, Marshall WR. Evaporation from drops, part ii. Chem Eng Prog 1952;48(3):173–80.

[39] Spalding DB. The combustion of liquid fuels. In: Symposium (international) on combustion. Vol. 4. 1953. pp. 847–864.

[40] Pang KM, Jangi M, Bai X-S, Schramm J. Evaluation and optimisation of phenomenological multi-step soot model for spray combustion under diesel engine-like operating conditions. Combust Theory Model 2015;19(3):279–308.

[41] Chomiak J, Karlsson A. Flame liftoff in diesel sprays. In: Symposium (international) on combustion. 26, (2):Elsevier; 1996, p. 2557–64.

[42] Yoshizawa A, Horiuti K. A statistically-derived subgrid-scale kinetic energy model for the large-eddy simulation of turbulent flows. J Phys Soc Japan 1985;54(8):2834–9.

[43] Xu L, Bai X-S, Jia M, Qian Y, Qiao X, Lu X. Experimental and modeling study of liquid fuel injection and combustion in diesel engines with a common rail injection system. Appl Energy 2018;230:287–304.

[44] Reitz RD. Modeling atomization processes in high-pressure vaporizing sprays. Atomisation Spray Technol 1987;3(4):309–37.

[45] Bravo L, Kweon C-B. A review on liquid spray models for diesel engine computational analysis. Technical Report, United States Army Research Laboratory; 2014.

[46] Zhang Y, Jia M, Liu H, Xie M, Wang T, Zhou L. Development of a new spray/wall interaction model for diesel spray under PCCI-engine relevant conditions. Atomization Sprays 2014;24(1):41–80.

[47] Ricart LM, Reltz RD, Dec JE. Comparisons of diesel spray liquid penetration and vapor fuel distributions with in-cylinder optical measurements. J. Eng Gas Turbines Power 2000;122(4):588–95.

[48] Jangi M, Solsjo R, Johansson B, Bai X-S. On large eddy simulation of diesel spray for internal combustion engines. Int J Heat Fluid Flow 2015;53:68–80.
[49] Nordin PN. Complex chemistry modeling of diesel spray combustion. Vol. 18. Chalmers University of Technology Sweden; 2001.
[50] Hadadpour A, Jangi M, Pang KM, Bai X-S. The role of a split injection strategy in the mixture formation and combustion of diesel spray: A large-eddy simulation. Proc Combust Inst 2019;37(4):4709–16.
[51] D'Errico G, Lucchini T, Contino F, Jangi M, Bai X-S. Comparison of well-mixed and multiple representative interactive flamelet approaches for diesel spray combustion modelling. Combust Theory Model 2014;18(1):65–88.
[52] Lu T, Law CK, Yoo CS, Chen JH. Dynamic stiffness removal for direct numerical simulations. Combust Flame 2009;156(8):1542–51.
[53] Hu S, Gong C, Bai X-S. Dual fuel combustion of N-heptane/methanol-air-EGR mixtures. Energy Procedia 2017;105:4943–8.
[54] Burke U, Metcalfe WK, Burke SM, Heufer KA, Dagaut P, Curran HJ. A detailed chemical kinetic modeling, ignition delay time and jet-stirred reactor study of methanol oxidation. Combust Flame 2016;165:125–36.
[55] Jangi M, Bai X-S. Multidimensional chemistry coordinate mapping approach for combustion modelling with finite-rate chemistry. Combust Theory Model 2012;16(6):1109–32.
[56] Solsjö R, Jangi M, Chartier C, Andersson O, Bai X-S. Lift-off and stabilization of n-heptane combustion in a diesel engine with a multiple-nozzle injection. Proc Combust Inst 2013;34(2):3031–8.
[57] Dempsey AB, Walker NR, Reitz R. Effect of piston bowl geometry on dual fuel reactivity controlled compression ignition (RCCI) in a light-duty engine operated with gasoline/diesel and methanol/diesel. SAE Int J Engines 2013;6(1):78–100.
[58] Bilger R, Stårner S, Kee R. On reduced mechanisms for methane air combustion in nonpremixed flames. Combust Flame 1990;80(2):135–49.
[59] Westbrook CK. Chemical kinetics of hydrocarbon ignition in practical combustion systems. Proc Combust Inst 2000;28(2):1563–77.
[60] Hadadpour A, Jangi M, Bai X-S. Jet-jet interaction in multiple injections: A large-eddy simulation study. Fuel 2018;234:286–95.